

Helium Adsorption in Silica Aerogel near the Liquid-Vapor Critical Point

Tobias Herman,* James Day, and John Beamish†

Department of Physics, University of Alberta, Edmonton, Alberta, Canada

(Dated: October 12, 2018)

We have investigated the adsorption and desorption of helium near its liquid-vapor critical point in silica aerogels with porosities between 95% and 98%. We used a capacitive measurement technique which allowed us to probe the helium density inside the aerogel directly, even though the samples were surrounded by bulk helium. The aerogel's very low thermal conductivity resulted in long equilibration times so we monitored the pressure and the helium density, both inside the aerogel and in the surrounding bulk, and waited at each point until all had stabilized. Our measurements were made at temperatures far from the critical point, where a well defined liquid-vapor interface exists, and at temperatures up to the bulk critical point. Hysteresis between adsorption and desorption isotherms persisted to temperatures close to the liquid-vapor critical point and there was no sign of an equilibrium liquid-vapor transition once the hysteresis disappeared. Many features of our isotherms can be described in terms of capillary condensation, although this picture becomes less applicable as the liquid-vapor critical point is approached and it is unclear how it can be applied to aerogels, whose tenuous structure includes a wide range of length scales.

I. INTRODUCTION

Fluid phase transitions can be drastically changed by confinement in small pores. Helium has a rich phase diagram and well-understood bulk behavior and is an ideal system in which to study these changes. Silica aerogels, with their tenuous structure and extraordinarily low densities, provide a unique opportunity to introduce impurities in a controllable way and so to address fundamental questions about how disorder, finite size effects and surfaces affect phase transitions and critical behavior. Recent work on the helium/aerogel system has provided insights into the role of disorder in a wide range of phase transitions. For example, the lambda transition for ^4He in aerogels^{1,2} remains sharp, but with a non-bulk critical exponent for superfluid density, while for ^3He aerogels suppress or even completely eliminate superfluidity^{3,4}, resulting in a zero temperature “quantum phase transition.” For ^3He - ^4He mixtures, the presence of 2% or even 0.5% silica (i.e. aerogels with porosity of 98% or 99.5%) has dramatic effects^{5,6,7} on the entire phase diagram, causing the phase separation curve to detach from the lambda line and stabilizing a region of dilute ^4He superfluid inaccessible in bulk mixtures.

The range of effects aerogels have on the various transitions reflects differences in their correlation lengths and in how the order parameter couples to the aerogels. In superfluid ^4He , the correlation length is very small and only approaches that of the aerogel structure very close to the lambda point. The correlation length in superfluid ^3He is much larger, comparable to aerogel length scales at all temperatures. In ^3He - ^4He mixtures, the aerogel strands couple directly to the order parameter (^3He concentration), in contrast to the much weaker coupling to the superfluid order parameters in ^3He and ^4He .

The liquid-vapor phase transition in porous media has considerable fundamental and practical interest. It is often described within the framework of capillary condensation since, in geometries like pores or channels, fluids

tend to condense more readily than in bulk. That is, liquid forms at pressures lower than the bulk saturated vapor pressure. This behavior is usually described by taking into account the energetics of liquid-vapor and liquid-solid interfaces (i.e. surface tension) and the depression of condensation pressure is fairly well-described by the Kelvin equation, even in very small pores⁸. Capillary condensation is characterized by very deep metastable states during adsorption and desorption, which leads to hysteresis along adsorption isotherms.

Although extracting pore size distributions for real porous media requires simplifying assumptions, the fundamental aspects of capillary condensation are well explained. However, near the liquid-vapor critical point (LVCP) this picture breaks down. Thermal fluctuations grow from atomic to macroscopic scale as the LVCP is approached and many thermodynamic properties diverge (e.g. the liquid-vapor interface thickness) or tend to zero (e.g. the surface tension). Close to the critical point, density fluctuations might exceed the size of the pores, raising the question of how the critical behavior responds to confinement. In bulk fluids, the liquid-vapor transition falls into the Ising universality class and deGennes^{9,10} suggested that fluids in porous media may provide a realization of the random field Ising model (RFIM). However, most measurements in pores and gels show slow dynamics¹¹, metastability and hysteresis and this complicated behavior makes it difficult to compare directly to theories of phase transitions in disordered media.

Experimental work on capillary condensation of near-critical fluids includes dense porous glasses such as CPG (controlled pore glass)^{12,13,14}. These studies show a slight narrowing in the phase separation curve, with the “vapor” branch shifted to higher densities than in the bulk fluid. In addition, the termination of this curve, sometimes referred to as the “capillary critical point,” is shifted to a temperature below the bulk LVCP. Despite the relatively well defined pore geometries of these systems there is no general agreement about how to picture

these systems near the LVCP. Aerogels provide an opportunity to study this transition in a very different medium, one without a well-defined pore shape. With their tenuous network of silica strands, it is hard to imagine a liquid-vapor meniscus with the uniform negative curvature usually associated with capillary condensation. On the other hand, aerogels could be the ideal system in which to study liquid-vapor critical behavior in the dilute impurity limit. However, a recent direct measurement of density fluctuations in carbon dioxide confined in aerogel¹⁵ showed little evidence for a diverging correlation length at the LVCP and thermal fluctuations may be less important than those introduced by the disorder in the aerogel structure¹⁶.

The first liquid-vapor experiments involving aerogels¹⁷ showed a reduced critical temperature for ^4He in a 95% porosity sample and a coexistence region which was dramatically narrowed (by a factor of ten). Below the critical point, isotherms appeared to have discontinuous density jumps between vapor and liquid-like phases and no hysteresis was observed. The surprisingly narrow coexistence curve, determined from heat capacity and isotherm measurements, could be fit using the bulk critical exponent. Measurements with N_2 ¹⁸ showed slow dynamic behavior (in density fluctuations in light scattering) and a coexistence curve that was also narrower than for bulk (although substantially broader than for ^4He). More recently, a low frequency mechanical pendulum technique was used to measure adsorption isotherms and study^{19,20} the liquid-vapor behavior of ^4He in a similar aerogel. The measurements were affected by very long thermal response times but showed finite isotherm slopes and hysteresis between filling and emptying, even near the critical point. The behavior was reminiscent of capillary condensation, rather than equilibrium coexistence and critical behavior. Our preliminary ultrasonic, acoustic resonator and isotherm measurements^{21,22,23,24,25} on neon and helium in aerogels also showed hysteresis and our phase separation curves were narrower than in bulk fluids, but substantially broader than the ^4He curve in Ref. 17.

Recently, computer models of fluid adsorption in aerogel have also reached a level of realism which allows direct comparison between experimental and simulated adsorption isotherms^{16,26}. These simulations were made using a lattice-gas model, with the aerogel structure produced by a diffusion-limited cluster-cluster aggregation algorithm. The use of the lattice-gas model allows the very large simulation volumes necessary for investigating low density aerogels. The simulations favor an interpretation without a macroscopic equilibrium phase transition near the bulk critical point and provide a picture of the liquid-vapor interface during adsorption in aerogel. The simulations show an interface with a range of curvatures, which becomes less distinct as the temperature is raised.

The liquid-vapor phase transition has not been systematically experimentally studied around the LVCP. While adsorption isotherms of low density aerogels at tempera-

tures far below the LVCP have shown how the isotherm shape changes with porosity²⁷, data near the LVCP are restricted to a single porosity (namely 95%). How hysteresis in the adsorption isotherms disappears as the temperature is raised has not been quantitatively studied for fluids in aerogel, and raises interesting questions about the effects of impurities on liquid-vapor critical behavior. The existence of equilibrium liquid-vapor transition for fluids in low density aerogels, necessary for there to be true critical behavior, is an open question. While there is little evidence for liquid-vapor critical behavior in denser media, as the concentration of impurities (i.e. aerogel density) is reduced this critical behavior may resurface.

In this paper, we describe a series of experiments on the isothermal adsorption and desorption of helium in silica aerogels of different densities. The aerogels were surrounded by bulk helium, but we used a capacitance measurement technique which allowed us to probe the helium density inside the aerogel directly. We controlled and varied the pressure, and thus the chemical potential, rather than admitting fixed amounts of helium. Thermal equilibration within aerogels was exceptionally slow; their tenuous microstructure suppressed convection and conducted heat very poorly. This slow equilibration was controlled by the heat of adsorption when fluid is added to (or removed from) the gel. Pressures equilibrated rapidly due to the aerogels' large permeability, but the heat of adsorption produced a temperature gradient which kept the fluid density within the gel from equilibrating until this heat had been conducted through the sample. We minimized equilibration times by cutting our samples as thinly as possible (less than 0.5mm), but the system could still take hours to equilibrate after a pressure step. Since there was no way to avoid this slow equilibration in monolithic aerogels, we monitored the pressure, bulk helium density and helium density inside the aerogel and waited at each point until all had stabilized. We then made detailed measurements to see how the isotherm shapes and hysteresis depended on aerogel density and how they evolved with temperature near the LVCP.

Our results show that hysteresis in adsorption isotherms persists to temperatures very close to the LVCP, and there is no sign of an equilibrium liquid-vapor transition once the hysteresis disappears. With aerogel samples with porosities between 95% and 98%, and isotherms taken at temperatures from 4.880K to helium's bulk critical point at 5.195K, we are able to analyze the evolution of adsorption isotherms with temperature and aerogel density. The shapes of our isotherms agree with simulation studies¹⁶, and recent experimental²⁰ work, but show no signs of the surprisingly narrow coexistence region¹⁷ seen in the first study published on helium condensation on aerogel.

II. EXPERIMENT DETAILS

A. Aerogel samples

Adsorption isotherms were collected for helium condensation in several aerogel samples. The two samples studied in detail had densities of $110 \frac{\text{kg}}{\text{m}^3}$ and $51 \frac{\text{kg}}{\text{m}^3}$ corresponding to porosities of 95% and slightly less than 98% respectively; throughout this paper they are referred to as aerogels “B110” and “B51.” These aerogel samples were synthesized in our lab from TMOS using the standard one-step base catalyzed method followed by supercritical extraction of the methanol solvent²⁸. Sample B51 was the lowest density sample that we could reliably get to gel using the one-step process — to go to lower densities (and thus higher porosities) one must use a two-step synthesis procedure²⁹. Data from a third sample, designated “U90,” are not presented in detail here since the aerogel was not made in our laboratory and its synthesis conditions are unknown. Its physical appearance resembled that of our other two samples, and it had a density of $90 \pm 25 \frac{\text{kg}}{\text{m}^3}$.

The aerogel samples were $\sim 0.5\text{mm}$ thick discs cut³⁹ from monolithic aerogel cylinders about 12mm in diameter and $\sim 2.5\text{cm}$ long. Because of the highly fragile nature of aerogels, great care had to be taken at all points to minimize any forces on the discs. Copper films were then deposited directly onto both faces of the aerogel discs by thermal evaporation through a 9mm diameter mask (deposited at 0.3–0.4 nm/sec to a thickness of $200 \pm 20\text{nm}$, as determined by quartz crystal thickness monitor). Empirically, metal did not seem to penetrate significantly into the aerogel and the copper film did not plug the pores as it would for a denser porous medium. The metal film acted as a continuous electrode, confirmed by electrical conductivity measurements. By patterning the electrodes directly onto to aerogel we ensured that any bulk fluid in the experimental cell could only influence our measurements through the capacitor’s fringe fields; it could not intrude directly between the capacitor plates.

The samples acted as parallel plate capacitors, but included significant effects from fringe fields (electric field lines which project from the edges of the capacitor) through the bulk helium in the cell. Since the measured capacitance depended on the details of all the electric field lines, it was affected by the environment outside as well as that inside the aerogel. This effect was clearly seen in the experiment — for a slice of aerogel of our dimensions, fringe fields caused the capacitance to deviate from the ideal infinite parallel plate capacitance by about 10%. The aerogel capacitors were also modelled using an electrostatic modelling program⁴⁰. The model calculations reproduced the magnitude of the fringe field effect seen experimentally³⁰.

B. Cell Design

There were three distinct modules to the cell, each with a single measurement function — a central piece and two endcaps. The center included a capacitive pressure gauge and an inlet capillary through which fluid could be admitted. One endcap measured bulk fluid density using a coaxial cylindrical capacitor with the bulk fluid acting as a dielectric between the plates. The other endcap was used to hold the aerogel sample for measurements of fluid density within the gel. Details of the experimental setup can be found in Ref. 30.

The aerogel lay in a shallow copper cup which made contact with the bottom electrode on the aerogel slice and was electrically connected to an isolated feed-through soldered into the cell. Contact to the top electrode was made by a patch of fine metal mesh — the patch acted as a very weak spring, holding the slice in place while ensuring good electrical contact to another feed-through. A typical aerogel sample had a capacitance of $C_0 \approx 2\text{pF}$. The experimental cell was designed to reduce stress on the sample, allowing us to work with weak, high porosity, aerogels.

The bulk density capacitor had a capacitance of $C_{\text{bulk}} \approx 35\text{pF}$. The outer plate was a 1cm length of 1.25cm diameter thin-walled stainless steel tubing; the inner plate was a 1cm long solid copper cylinder machined to fit inside the tubing with a slight gap between the two. The two plates were separated by eight small dabs of epoxy — the epoxy held the plates apart, but filled a negligible amount of the inter-plate volume (less than 2%).

The *in situ* pressure gauge was necessary to obtain sufficient precision and reproducibility for our experiments. The gauge was constructed after the design of Straty and Adams³¹, and consisted of a 0.2mm thick hardened beryllium-copper diaphragm whose deflection influences the separation of two parallel brass plates. The gauge was calibrated for each data run using a room temperature pressure gauge⁴¹.

The cell was mounted on a liquid helium cryostat, with cooling power provided by helium exchange gas. Temperature was controlled using a calibrated Germanium resistive thermometer and 200Ω thick film resistive heater mounted directly on the cell body. Cell temperature was controlled to $\pm 50\mu\text{K}$ with long term drift also of about $\pm 50\mu\text{K}$.

C. Data Collection

Most capacitance data from aerogel B110 were obtained using a manually balanced capacitance bridge. Since we did not use a low temperature reference capacitor, the bridge’s resolution and drift limited the experimental resolution to about 1 part in 10^5 . Later data, including all data on aerogel B51, were collected using an

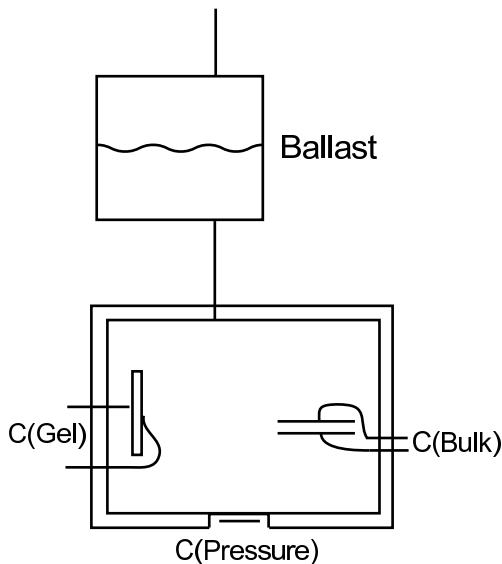


FIG. 1: A schematic of the low temperature portion of the setup used to measure aerogel capacitance during adsorption of helium in silica aerogel.

automated capacitance bridge⁴² with much higher resolution.

Helium was admitted to the cell using two different methods. In the first method, helium was directly admitted to the cell from a room temperature gas handling system through a mass flow controller. This ensured a continuous flow into the cell at a well controlled rate, but even the slowest rate of flow was too fast to allow for relaxation within the aerogel. To allow for thermal equilibration, the flow controller had to be shut off and the system allowed to relax until the fluid density in the aerogel stopped changing. Most data from sample B110 were taken in this manner.

For collecting data on aerogels B51 and U90, a low temperature ballast volume was mounted about 33cm above the cell for collecting equilibrated points; the setup is shown schematically in Fig. 1. Helium was admitted to the ballast and the pressure of the system was then controlled by adjusting the temperature of the ballast volume. The ballast and cell were connected by a ~ 50 cm length of 0.2mm i.d. CuNi capillary and their temperatures were controlled independently. When the ballast held coexisting liquid and vapor, a small step in the ballast temperature would change the equilibrium vapor pressure of the helium in the ballast, and consequently change the pressure in the sample cell.

This latter method is directly analogous to simulation studies of hysteretic adsorption of fluids in which the chemical potential is gradually incremented and the response of the fluid density is monitored. Using this pressure stepping technique, we ensured that we remained along the outside edge of any hysteresis loops. On the

other hand, if volumetric bursts were added to, or removed from, the system, an unknown degree of local heating or cooling could have occurred within the sample. Thus, precise knowledge would be lost about where the system was within the hysteretic region. When a system is not governed by metastability the methods should give identical results, but when hysteresis is present the current state of the system depends on all the states it occupied along the way.

Using the pressure regulation ballast allowed us to automate small pressure steps along the adsorption isotherm and required no additional helium input from the gas handling system outside the cryostat. Our technique worked well for isotherms with finite slopes, but it only produced a few points along very flat isotherms (i.e. isotherms where the aerogel sample filled with liquid over a narrow pressure range) whereas the dosing technique would have allowed a higher density of points. For B110 there was no problem obtaining enough points along the hysteresis loop of the isotherm, but for B51 the isotherms were so flat that they would fill or empty completely over a pressure range spanned by only two or three data points.

The resolution and drift of the manual capacitance bridge were the limiting factors in the earlier isotherms, but the resolution of the automated capacitance bridge is about an order of magnitude better than the experimental noise. For most of the data therefore, resolution was set by temperature control. The resolution of the bulk helium density capacitor is better than $\pm 0.01 \frac{kg}{m^3}$. The aerogel helium density resolution is somewhat sample dependent, but always better than $\pm 1 \frac{kg}{m^3}$. Both the bulk and aerogel helium density capacitances show slight shifts with temperature which contribute an additional error of less than $0.5 \frac{kg}{m^3}$ over the temperature range of these data. The method we used for converting aerogel capacitance to helium density also introduced errors on the order of those due to electrical noise.

Since the sample was mounted with its axis horizontal, there was a gravitational pressure head of up to $60\mu\text{bar}$ across the 1.2cm diameter sample. The uncertainty and drift in cell and ballast temperatures ($\pm 50\mu\text{K}$), and the slope of the coexistence curve of helium near its critical point ($\sim 1.5\text{bar}/\text{K}$) combined to restrict our experimental pressure resolution to about $70\mu\text{bar}$. The similar size of these two factors meant that both the sample dimensions and temperature control would have to be changed to improve experimental resolution significantly.

III. RESULTS

A. Bulk Helium Density

The bulk helium capacitor was calibrated by using the measured capacitance and literature values³² for the density of helium liquid and vapor at saturated vapor pressure at 4.400K. These values were used to fit the helium

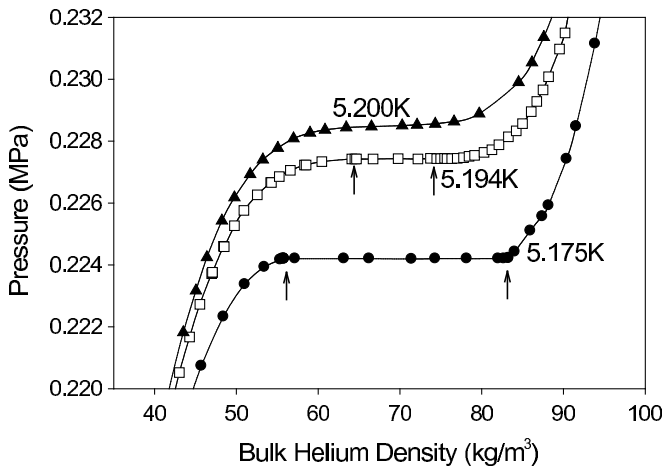


FIG. 2: Isotherms for bulk helium near the critical temperature of 5.1952K. Below T_c there exists a region of two-phase coexistence where the isotherm is completely flat, indicated by the arrows along the isotherms at 5.175K and 5.194K. Above T_c this flat region is replaced by an inflection point.

density (ρ_{bulk}^{He}) to an expression of the form:

$$\rho_{bulk}^{He} = A(C - C_0^{eff}) \quad (1)$$

where C was the measured capacitance and A and C_0^{eff} were adjustable constants which were recalculated for each data run. The bulk helium capacitor had a slight background temperature dependence so a small empirical temperature correction was added to minimize deviations from literature values at higher temperatures. A comparison between densities calculated from our experimental data and values extracted from the NIST Chemistry WebBook³² showed deviations less than $0.3 \frac{kg}{m^3}$ for temperatures from 4.400K to just below the bulk critical temperature of helium (5.195K). Since bulk helium density is only used to account for the effect of the aerogel capacitor fringe fields, this degree of accuracy is sufficient.

Using this calibration, bulk pressure-density isotherms were collected. Three examples of bulk isotherms are shown in Fig. 2, two below T_c (which was empirically determined to be 5.1952K on our thermometer calibration) and one above it. For the $T < T_c$ isotherms a distinct coexistence region is marked by arrows. The width of the two-phase coexistence region shrinks as the critical temperature is approached; above T_c there is no coexistence and isotherms are single smooth curves with an inflection point at the critical density. Even when the onset of coexistence was a little unclear on a pressure-density plot, such as the $T=5.194K$ isotherm in Fig. 2, it was obvious when looking at the time dependence of the data during a constant flow adsorption isotherm — once coexistence was reached the capacitance of the bulk helium capacitor remained constant for a long time, until the liquid-vapor meniscus in the cell reached the bulk helium capacitor. From the slopes of supercritical isotherms it is

also possible to determine the compressibility of bulk helium, with flat isotherms below the LVCP corresponding to a diverging compressibility.

B. Helium Density in Aerogel

The effective dielectric constant of a porous medium depends on the dielectric constant of the matrix, that of the fluid in its pores, and the geometry of the system. With knowledge of those three factors it is possible to calculate an effective dielectric constant³³. Since aerogel acts as a dilute impurity, it turns out that there is little deviation from a linear relationship between fluid density and capacitance. When a single fluid phase is present there is a nonlinear term in the dielectric constant of the aerogel which depended on the aerogel porosity (ϕ) and the fluid dielectric constant (ϵ_{He}). This term, proportional to $(1 - \phi) * (\epsilon_{He} - 1)$, was negligible in our measurements since we were using 95% and 98% porous gels and the dielectric constant of helium is less than 1.05 at the temperatures and pressures used in our experiments. When phase separated liquid and vapor were present inside the aerogel, more assumptions had to be made since the geometry of the liquid-vapor interface was not known. However, deviations from linearity were still smaller than 3%³⁰, less than both the experimental variations between runs and the features we were investigating.

There are actually three contributions to the measured capacitance of the aerogel sample: the capacitance of the empty aerogel (C_0), the capacitance added by the helium in the aerogel (C_{gel}^{He}), and the capacitance added by the bulk helium in the fringe fields outside of the aerogel sample (C_{bulk}^{He}):

$$C_{total} = C_0 + C_{gel}^{He} + C_{bulk}^{He} \quad (2)$$

To find the density of helium in the aerogel these three factors were determined separately, using an adsorption isotherm taken at 4.400K to determine their relative sizes. The capacitance of the aerogel was measured when empty (C_0), when full with liquid but surrounded by bulk vapor (C_A), and when full with liquid and surrounded by bulk liquid (C_B) — see Fig. 3 for details. As the aerogel fills with helium, capacitance increases until point “A,” where the aerogel is completely filled with liquid. The spike of noise in pressure at point A is related to momentary temperature control problems in the cell as bulk liquid begins to condense into the cell. As the bulk liquid meniscus moves up over the aerogel sample (i.e. between points “A” and “B”) the capacitance increases due to fringe fields in the bulk helium, not due to the helium density within the sample. By quantifying these fringe effects it is possible to correct the capacitance data for the small spurious shifts due to changes in bulk fluid density in the cell.

We assume that far from the LVCP the density of liquid helium in aerogel is equal to that of bulk liquid helium; while there may be a slight enhancement of he-

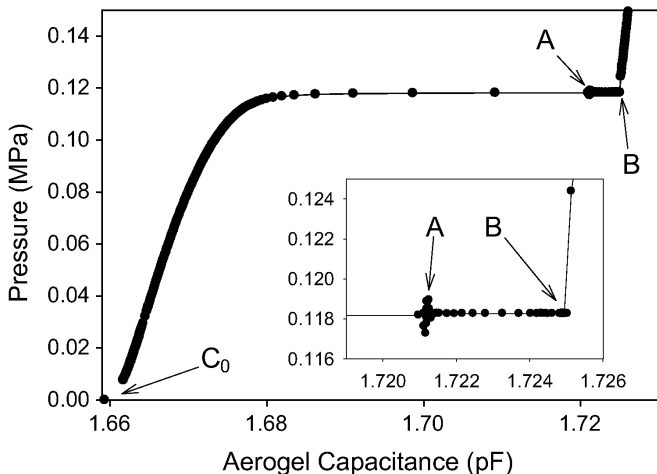


FIG. 3: Continuous flow helium adsorption isotherm for sample B110 at 4.400K. C_0 is the capacitance of the empty aerogel, point “A” corresponds to the aerogel being full of liquid coexisting with bulk vapor outside the gel, and point “B” corresponds to a full gel surrounded by bulk liquid helium. The inset enlarges the region where fringe field effects are most obvious.

lium density due to denser layers adsorbed on the silica strands, it will not be important far from the critical point. The first layer of helium adsorbed on the aerogel surface accounts for less than 8% of the open volume in the aerogel (for 95% porosity aerogel). Even if we assume that the first layer is 25% denser than bulk liquid helium, then the total helium density of the system will only be enhanced by about 2% far from the LVCP.

Using the three points along the 4.400K isotherm mentioned above, and assuming that helium density at 4.400K in aerogel is identical to bulk helium density, it is possible to fit the density of the helium to an expression of the form:

$$\rho_{gel}^{He} = D \left(C_{gel} - C_0 - \frac{\rho_{bulk}}{E} \right)$$

where “D” reflects the sensitivity of the capacitor to the density of helium in the aerogel and “E” reflects the effects of the fringe fields (i.e. the influence of the environment surrounding the gel, which must be subtracted from the signal). The constants (C_0 , D, and E) must be determined for each run since even a small change in position of the sample can have significant effects on the density calibration. When bulk capacitance and aerogel capacitance were measured simultaneously it was simple to account for the fringe effects. However, occasionally bulk data were not available, so the density for bulk helium at SVP was used to approximate ρ_{bulk} (bulk vapor density, since our isotherms were taken below bulk saturation).

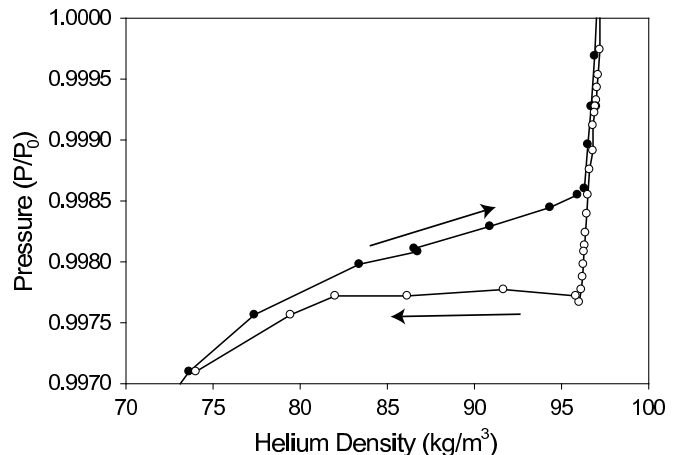


FIG. 4: Equilibrated isotherm at 5.100K in aerogel B110. This isotherm displays a well defined hysteresis loop — thermal equilibrium of points along the hysteresis loop was very slow, while points that did not lie along the hysteresis loop equilibrated in a few minutes. Points along the adsorption isotherm are shown as solid symbols, while points along the desorption isotherm are shown as open symbols.

C. Thermal Equilibration

Aerogels are truly phenomenal thermal insulators, a fact which leads to very slow thermal equilibration within samples. By using the thinnest samples (only a few hundred micrometers thick) we minimized the thermal equilibration time. To ensure that we were measuring rate-independent isotherms, we directly monitored the equilibration of helium density during adsorption and desorption.

One example of an equilibrated isotherm is shown in Fig. 4 for helium in aerogel B110 at 5.100K. Figure 5 shows the response at 5.100K to a change of 1mK in ballast temperature. The data in Fig. 5 were taken during a data run subsequent to that in Fig. 4. While the step in ballast temperature was effectively instantaneous and the cell pressure and bulk helium density responded completely within a few minutes, the density of helium in the aerogel sample took hours to equilibrate. This is probably due to the slow thermal equilibrium within the aerogel; while the aerogel is highly permeable to helium, convection is suppressed by the aerogel strands. Equilibration during emptying took about twice as long as filling, as shown in Fig. 6.

The relaxation in aerogel B51 was even slower than in aerogel B110; a direct comparison of emptying steps for the two is also shown in Fig. 6. The step along the B51 desorption isotherm corresponded to a change in $T_{Ballast}$ of only 0.1mK, as opposed to the 1.0mK change shown for aerogel B110. Since the change in helium density in aerogel B51 is driven by a much smaller temperature change in the ballast, the pressure and temperature gradients across the sample during desorption are smaller in aerogel B51. For a given density change the amount of

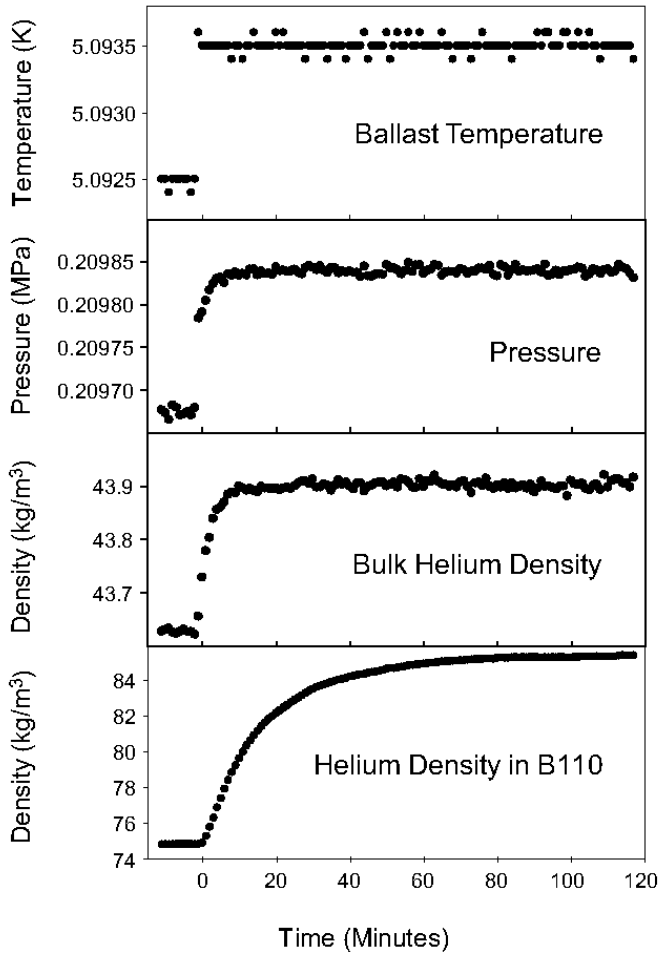


FIG. 5: Equilibration at 5.100K following a 1mK step in ballast temperature.

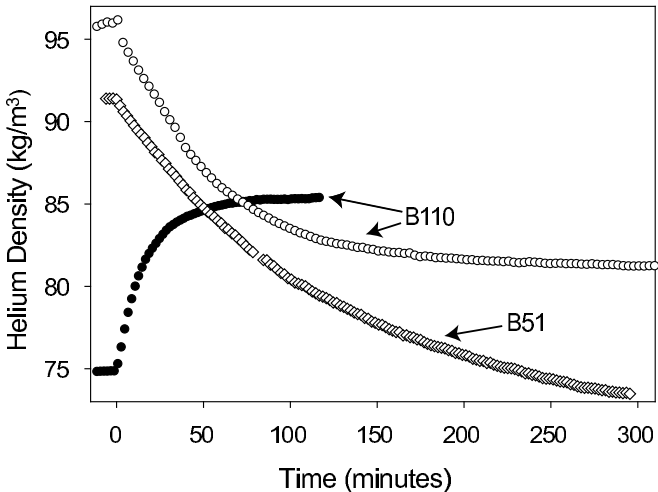


FIG. 6: Comparison between relaxation in aerogels B110 (filling and emptying) and B51 (emptying) at $T=5.100\text{K}$. The data shown here corresponds to ballast temperature steps of $\pm 1\text{mK}$ for B110 and -0.1mK for B51.

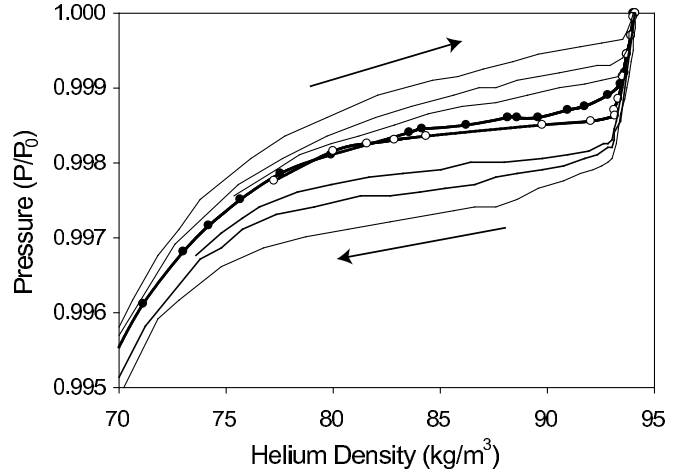


FIG. 7: Isotherms for helium adsorption in aerogel B110 at 5.140K showing three continuous filling rates and also equilibrated points. The time to complete the isotherms, from the outer loop to the inner loop, were 1.5hours, 2.5hours, and 5hours. The equilibrated points, shown as the innermost loop, were collected over about 10 hours.

latent heat which must be supplied during desorption is approximately the same in B51 and B110, so the smaller temperature gradient present in B51 results in slower relaxation. In practical terms, this means that the equilibration time is inversely related to the slope of the adsorption isotherm — the flatter the isotherm, the slower the equilibration at each pressure.

Even at the slowest rates possible with our flow controller, continuous flow adsorption isotherms did not allow for thermal equilibration along hysteretic isotherms. The effects of filling rate are illustrated in Fig. 7 for isotherms taken at 5.140K in B110. The loop remained when the density was allowed to equilibrate at each point, but the size and shape of the continuous flow loops depended sensitively on the filling and emptying rates. The effect of filling rate was greater for the lower temperature isotherms while above bulk T_c equilibration was relatively fast and there was no hysteresis during continuous flow measurements.

IV. ADSORPTION ISOTHERMS

Adsorption isotherms were collected in aerogels B110 and B51 over similar temperature ranges; isotherms are shown for $T=4.880\text{K}$ and $T=5.150\text{K}$ in Figs. 8 and 9, which also include the corresponding measured isotherms for bulk helium.

Given the similar synthesis conditions, the physical microstructure of the gels should be very similar, leading to adsorption isotherms sharing many characteristics. At the temperatures shown here both samples exhibited hysteresis loops — these loops remained resolvable until quite near to the bulk critical temperature. The low

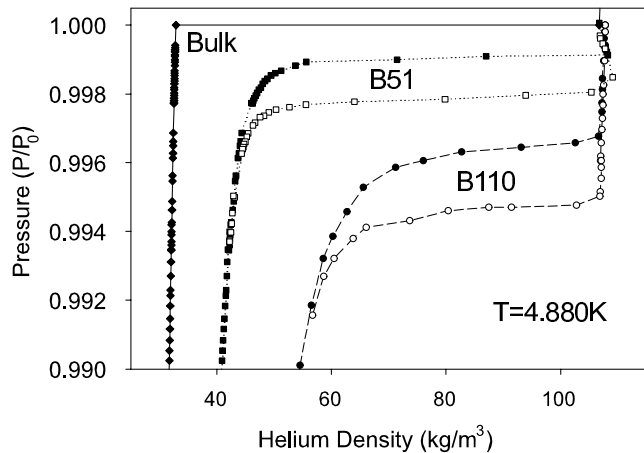


FIG. 8: Comparison between isotherms in aerogels B110 and B51 at $T=4.880\text{K}$

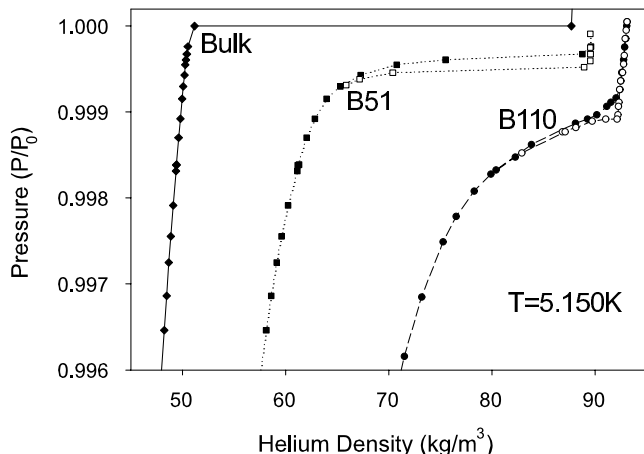


FIG. 9: Comparison between isotherms in aerogels B110 and B51 at $T=5.150\text{K}$

density sides of the adsorption isotherms curve smoothly into the hysteresis loops, making it difficult to precisely identify the onset of capillary condensation or define “vapor branches” for the isotherms. On the other hand, the high density sides of the isotherms had sharp transitions, allowing one to pinpoint the completion of capillary condensation with more precision.

However, there are also significant differences between adsorption isotherms in the two aerogels. In aerogel B51 the hysteresis loops occur closer to saturated vapor pressure (P_0) and cover a larger density range. The low density portion of the adsorption isotherms in B51 shows less density enhancement before the onset of capillary condensation — the less dense medium perturbs the helium density less from its bulk value. Similarly, the density enhancement when the gel is full (at 5.150K) is smaller in B51. Far from the critical point we assumed that the aerogel strands only perturb the density of the layer of he-

lium directly adjacent to the silica strands, but by 5.150K the system is close enough to the LVCP that the liquid-vapor interface has become less distinct and the fluid is very compressible. In this temperature region, perturbations in fluid density caused by the silica strands propagate further into the fluid.

The evolution and disappearance of the hysteresis loop as temperature is raised is also very different in these two samples. In B110 the loop disappears between 5.150K and 5.160K ($\sim 40\text{mK}$ below T_c), while in B51 it disappears between 5.170K and 5.180K ($\sim 20\text{mK}$ below T_c). Thus, the temperature difference between the point at which the hysteresis loop closes and the bulk T_c is roughly proportional to the aerogel density. The manner in which the loops close also differs. The hysteresis loop in sample B51 covers a smaller pressure range as the temperature is raised, but its shape does not change drastically. Sample B110, on the other hand, exhibits a hysteresis loop that seems to “zip” closed as the temperature is raised.

A. Helium in Aerogel B110

Sample B110 had a porosity close to the aerogel used by Wong and Chan in their work near the liquid-vapor critical point¹⁷ and very close to that used by the Grenoble group²⁰. We have equilibrated adsorption isotherms for sample B110 at temperatures from 4.880K to above the bulk critical temperature. At temperatures far below the LVCP, these isotherms show large hysteresis loops, which gradually shrink as the temperature is raised, until (at about 5.155K) they finally disappear. The hysteresis covers a large density range — much wider than the coexistence curve mapped out by Wong and Chan¹⁷ close to the LVCP — but are narrower than the bulk helium coexistence curve. For all loops, both adsorption and desorption branches have finite slopes; there are no isotherms that exhibit the flat coexistence regions seen in bulk helium.

The evolution with temperature of the hysteresis loops in B110 is shown in Fig. 10 — they shrink and become more triangular as the temperature is raised. The high density end of the loop remains well defined, especially along the desorption branch, but the hysteresis loop becomes less and less distinct at the low density end. The loop transforms from a roughly rectangular shape to a triangle until, at higher temperatures, it completely disappears (Fig. 11). While the hysteresis loop is still distinct at 5.150K , by 5.155K any loop is too small to resolve. The slight difference between the adsorption and desorption isotherms at 5.155K and 5.165K in this figure is a measure of the resolution and drift in our system — there does not appear to be any distinct loop as there was for the lower temperatures.

Since the mechanism for hysteresis in aerogel is not known, the disappearance of a hysteresis loop above 5.150K need not imply the disappearance of distinct pore

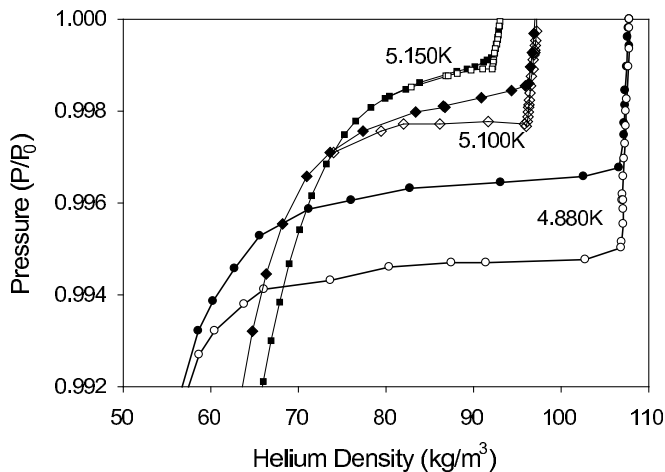


FIG. 10: Three isotherms in aerogel B110 at temperatures: $T=4.880\text{K}$, 5.100K , and 5.150K .

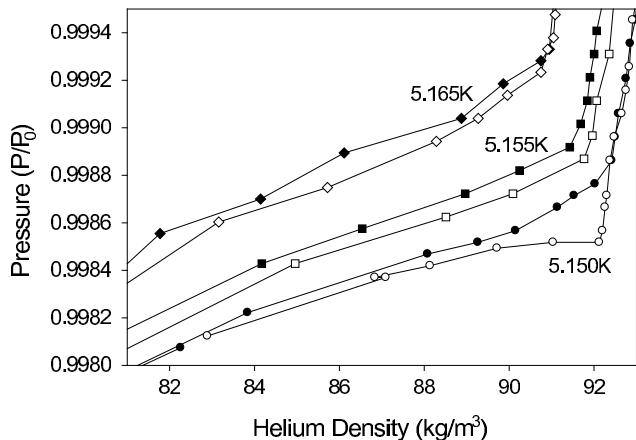


FIG. 11: Isotherms in aerogel B110: $T=5.150\text{K}$, 5.155K , and 5.165K . The data have been shifted to make this figure clearer — the $T=5.155\text{K}$ pressure data have been shifted by $-0.0002 P/P_0$ while the $T=5.150\text{K}$ pressure data have been shifted by $-0.0004 \frac{P}{P_0}$.

liquid and pore vapor phases. A fairly sharp kink at the high density side of the isotherm remains after hysteresis has disappeared. The eventual disappearance of this kink at some temperature above the disappearance of hysteresis but below the bulk critical temperature may be an indication of the disappearance of a distinct “pore liquid” phase.

B. Helium in Aerogel U90

We have also collected a series of isotherms on another aerogel sample, designated “U90,” with a density of about $90 \pm 25 \frac{\text{kg}}{\text{m}^3}$. Data were collected using the improved system, including the pressure regulation ballast. A single isotherm from this sample is included in Fig. 12.

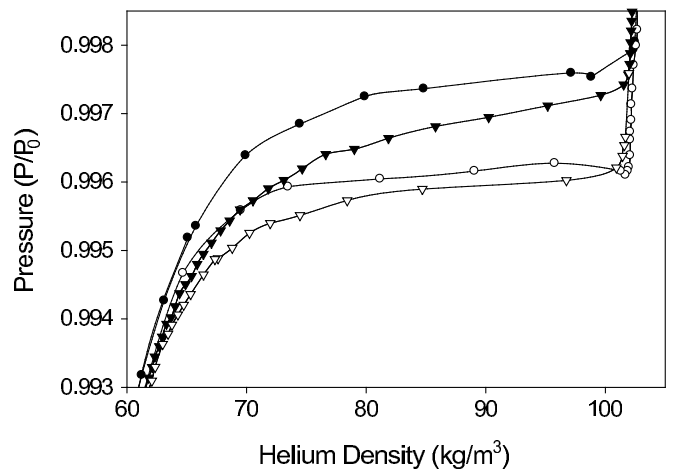


FIG. 12: Isotherms at 5.000K in aerogels B110(circles) and U90(triangles). The B110 data were collected manually while U90 data were collected using the automated system incorporating the pressure regulation ballast.

The adsorption and desorption isotherms in aerogel U90 were very similar to those in B110, including their temperature dependence.

C. Helium in Aerogel B51

Sample B51 had a density of $51 \frac{\text{kg}}{\text{m}^3}$, corresponding to a porosity of slightly less than 98%. Capillary condensation occurred at higher relative pressures than in the denser gel and the gel filled (or emptied) over an exceptionally narrow pressure range. Isotherms at 4.880K and 5.150K were shown earlier (Fig.’s 8 and 9). A single isotherm at 5.150K is shown in greater detail in Fig. 13. This can be compared to the 5.100K isotherm for B110 (Fig. 4). Most of the points along the 5.150K isotherm have been allowed to relax completely, although there was a single point, marked by an asterisk (*) in Fig. 13, that had not quite equilibrated.

Figures 14 and 15 show the evolution of the hysteresis loops with temperature. All isotherms are constructed from equilibrated points except the 4.880K isotherm — because of the extremely slow thermal equilibration within sample B51, it was not practical to wait for the points along the flattest region of the hysteresis loop to completely equilibrate at this one temperature. The hysteresis loops extend over a larger range of densities than in B110 but the aerogel fills or drains almost entirely in a single $\sim 100\mu\text{bar}$ pressure step. Hysteresis is still resolvable in the isotherm at 5.170K , although the precision of our pressure control is barely good enough (a few parts in 10^5) to resolve the loop. At 5.180K no hysteresis was seen. A number of points along the higher temperature isotherms showed a slow drift that could sometimes be comparable to the density change seen during that isotherm’s step. This is an indication that at such tem-

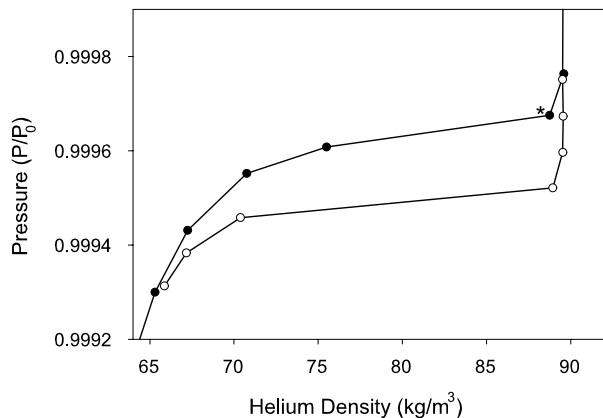


FIG. 13: Adsorption isotherm in aerogel B51 at $T=5.150\text{K}$. The only point in the plot which does not represent a fully relaxed state is indicated by the asterisk(*). Note that this loop is only a few times wider than our pressure resolution.

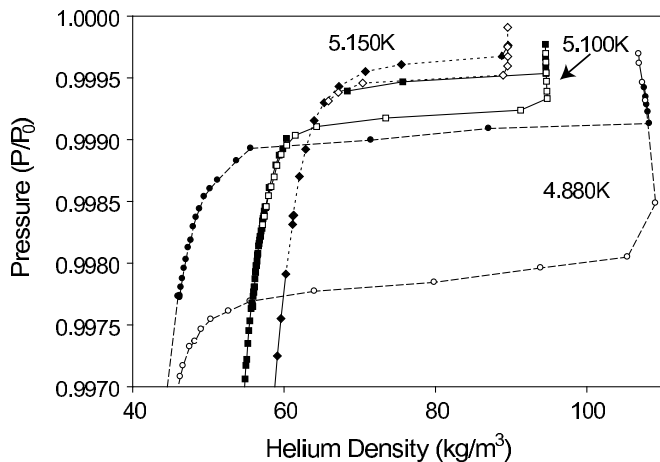


FIG. 14: Three isotherms in aerogel B51: $T=4.880\text{K}$, 5.100K , and 5.150K . The data along the 4.880K hysteresis loop is slightly out of thermal equilibrium along the flattest sections.

peratures the isotherms are *very* sensitive to cell temperature and pressure and we have reached the limits of our ability to control the system.

V. DISCUSSION

Previous measurements^{17,18,20} of liquid-vapor behavior have been made using aerogels with similar density to our sample B110 ($110 \frac{\text{kg}}{\text{m}^3}$, 95% porosity) and we can compare our results to those experiments. In this aerogel, our isotherms (Figs. 10 and 11) have nearly rectangular hysteresis loops far from the LVCP, but these become more triangular at higher temperatures. The loops finally disappear about 40mK below the bulk LVCP. All isotherms have non-zero slopes, in contrast to the flat

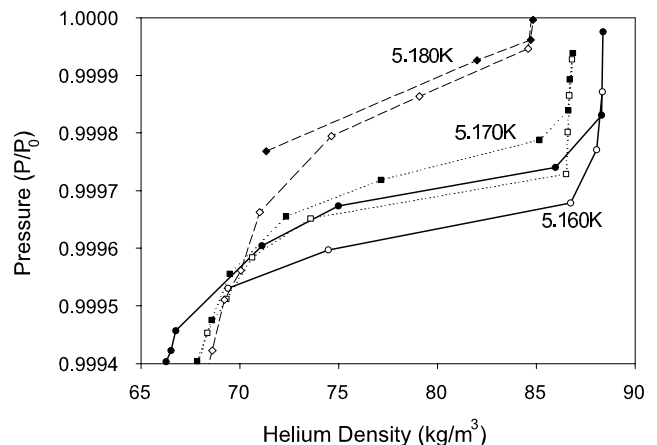


FIG. 15: Three isotherms in aerogel B51: $T=5.160\text{K}$, 5.170K , and 5.180K . Some points have been eliminated from the isotherm at 5.180K because they appeared to drift over time, indicating that we are operating at the limit of resolution for this system.

region associated with liquid-vapor coexistence in bulk helium (e.g. in Fig. 9). The onset of capillary condensation along the isotherms is gradual, making it impossible to unambiguously identify a low density fluid phase in the aerogel that is analogous to bulk vapor.

Gabay *et al.*^{20,34} used a mechanical oscillator to measure the helium density while isothermally flowing helium at different rates into or out of a similar aerogel. The hysteresis they observed depended on the flow rate, but was significant even for filling times as long as 64 hours. Their highest temperature hysteresis loops, at 5.140K , closely resemble those shown in Fig. 7. Our measurements show that this hysteresis persists in the static limit, implying that there are metastable thermodynamic states for helium in aerogel, even very near the bulk critical point. The rate dependence they observed is consistent with our long equilibration times, given their larger sample dimensions (1cm versus our 0.5mm). They also found that the isotherms always had finite slopes, in agreement with our measurements.

Wong and Chan, on the other hand, saw qualitatively different behavior¹⁷ near the LVCP of helium. They measured heat capacity along isochores and used the temperatures of the peaks to map out an extremely narrow coexistence curve near the LVCP, with the liquid branch shifted to *lower* density than bulk liquid in contrast to our measurements. They supplemented these measurements with several adsorption isotherms which had flat regions consistent with coexistence, and reported no hysteresis. Their isotherm measurements had limited pressure resolution, so would not have resolved the smallest slopes we observed. The absence of hysteresis in these isotherm is puzzling, but could reflect differences in how our samples were filled. They used the more common method in which known quantities of gas are admitted

in bursts and then let come to equilibrium — in essence stepping density rather than pressure. However, this can cause significant local heating as the gas condenses into the sample. When condensation occurs over a very narrow pressure range (as it does in aerogels near the critical point) a local temperature jump of even a few millikelvin would correspond to relative pressure shifts larger than the width of a hysteresis loop itself. The system would then relax along a different thermodynamic path and might not end up in the same metastable state it would reach if the chemical potential was isothermally changed in steps, as in our measurements, or continuously, as in Gabay *et al.*'s work. At lower temperatures, all techniques show hysteretic adsorption loops that cover a relatively wide density range, like the 4.880K data shown in Fig. 10^{27,34}.

The very narrow coexistence curve that Wong and Chan deduced from their heat capacity measurements was a surprising result. Neither we nor Gabay *et al.* were able to find either a true coexistence region or any features in our isotherms that would produce such a narrow curve. In addition to the method used to admit helium, there are several differences between the experiments which may be relevant. Both our cell and that of Gabay *et al.* had large open volumes, so the aerogel was always in contact with a substantial reservoir of bulk helium; Wong and Chan's cell had much less bulk volume. Our measurements and those of Gabay *et al.* were done isothermally; Wong and Chan's heat capacity measurements followed isochores. These differences mean that less helium was adsorbed or desorbed following a temperature step in their isochoric measurements than following a pressure step in our isotherms. However, even with no bulk helium present, a temperature step produces gradients in temperature and thus in pressure, resulting in an internal redistribution of helium within the aerogel, with similar long equilibration times. Since our sample dimensions were comparable to those in Wong and Chan's heat capacity measurements (about 0.25mm thick in their case), their samples probably had similarly long time constants, up to several hours. This makes interpretation of AC heat capacity measurements difficult, since only a very thin layer of helium near the surface of the sample would respond even at a heater frequency as low as 0.1 Hz.

Although our sample density is similar to that used by Wong and Chan, the liquid-vapor phase behavior could be sensitive to small differences in porosity or microstructure. However, we made measurements in another aerogel, U90, with similar density ($90 \frac{kg}{m^3}$) but synthesized elsewhere and Fig. 12 shows that the behavior at 5.000K is essentially the same as the behavior of B110 (as was the evolution of the isotherms with temperature). Thus, two different gels with similar densities, but from different sources, showed remarkably similar behavior. This supports the position that it is unlikely that any small structural differences between our samples and that of Wong and Chan could account for the dramatically dif-

ferent behavior observed in our experiments.

Our measurements on sample B51 ($51 \frac{kg}{m^3}$, 98% porosity) show how the shape and temperature dependence of adsorption isotherms depend on aerogel porosity, as summarized in Figs. 8 and 9. As expected, the effects of the aerogel on helium's liquid-vapor behavior become smaller as the density of the aerogel is reduced. Isotherms in the more porous gel (B51) resemble those in B110, but condensation occurs over a narrower pressure range, closer to bulk saturation. Hysteresis loops extend over a larger density range and persist to even higher temperatures, finally disappearing about 20mK below the bulk critical temperature. Perhaps more significantly, the shape of the hysteresis loops does not change as the LVCP is approached (Figs. 14 and 15); they remain rectangular, in contrast to the denser aerogel where they become triangular. The low density onset of condensation is sharper, but still rounded, and isotherms have a smaller, but non-zero slope at all temperatures. Capillary condensation begins at lower densities in the less dense aerogel, reflecting the smaller perturbation of the helium vapor by the silica strands. The enhancement of the liquid phase's density is smaller, but significant near the LVCP where it is more compressible (Fig. 9). Measurements by Tuliemi *et al.*²⁷ have also shown that aerogel density affects the shape of isotherms far from the critical point — they become sharper and flatter in high porosity aerogels.

Most papers on the liquid-vapor transition in porous media include plots of "coexistence curves." Exactly what features to include in such a plot, and even how to define those features, is somewhat arbitrary; however, once the plot is constructed it does allow for quick comparison to other experiments and to bulk fluid. To this end, in Fig. 16 we plot "coexistence curves" for helium in aerogels B110 and B51. When hysteresis loops are present, their closure points (which are always within the accompanying uncertainty of any "kinks" in the adsorption isotherm) are used to mark the onset and completion of condensation in the aerogel. When there is no hysteresis, we cannot identify a distinct low density feature, but over a limited temperature range there is still a kink which may indicate the end of capillary condensation and is a possible marker for the high density "liquid" branch of a coexistence curve. Figure 16 compares these curves for our high and low density aerogels, B110 and B51. The effective coexistence curves in both aerogels are narrower than for bulk helium and are shifted to higher densities. The changes are most significant for the denser aerogel, B110, but the curve is not nearly as narrow as Wong and Chan's coexistence curve for a similar porosity aerogel. The narrowing of the B110 curve is, however, similar to that previously seen for nitrogen¹⁸ and neon³⁰.

The behavior of fluids in pores near the liquid-vapor critical point has often been discussed in terms of a "capillary critical point" but there are a variety of definitions of this point^{12,13,35}. It is sometimes assumed to be the temperature where hysteresis disappears; in other work

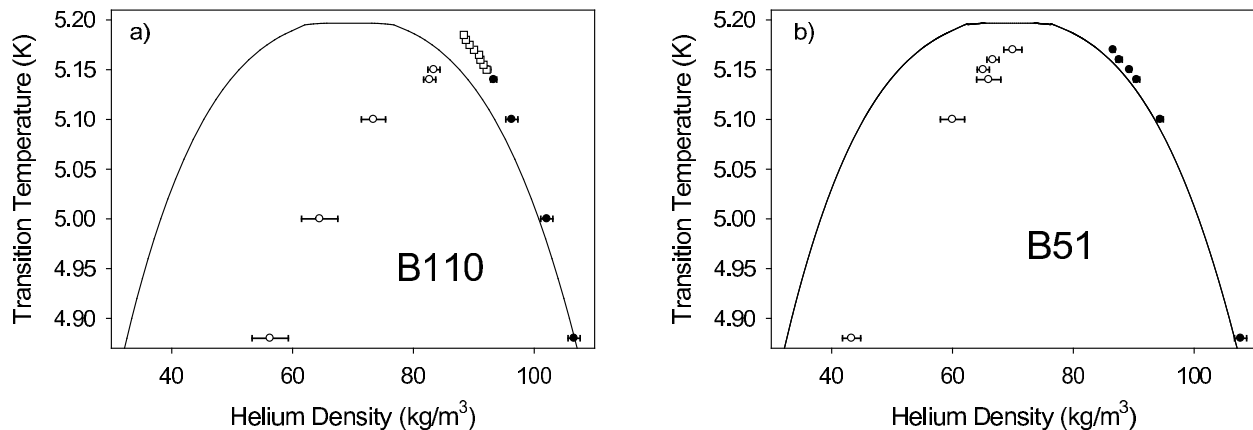


FIG. 16: Effective “coexistence curves” for helium in aerogel B110 and B51 plotted using the closure points of hysteresis loops (circles) as markers for the high and low density phases. In aerogel B110 additional data (squares) are included which may indicate the completion of capillary condensation at temperatures above the disappearance of hysteresis. Where error bars are not visible, they are smaller than the data symbols.

it is thought of as a more fundamental thermodynamic point which plays the same role as the liquid-vapor critical point in bulk fluids. In the former case, properties like surface tension are usually assumed to remain bulk-like. In the latter case, they may exhibit power law behavior close to the capillary critical point. In our measurements, the disappearance of hysteresis does not correspond to a true critical point since, for example, the fluid’s compressibility does not diverge at this temperature (the isotherm slopes do not approach zero). Well below the critical point, the isotherms become very flat, but the hysteresis prevents us from measuring the equilibrium compressibility to see if it diverges at some lower temperature. It is clear that our isotherms and “coexistence curves” like Fig. 16 cannot be analyzed in terms of equilibrium critical exponents, nor can we assign unique “capillary critical points” for helium in our aerogels.

Although we cannot access the equilibrium states of the system while it exhibits hysteresis, the simulations of helium condensation in 95% porosity aerogels^{16,26} can probe the energetics of states within the hysteresis loop. The fluid density in the equilibrium states showed a discontinuous jump in fluid density at a single value of chemical potential as one would expect with liquid-vapor coexistence. However, when the simulations raise and lower the chemical potential to fill and empty the aerogel (the analog of us varying the pressure in our measurements) they also show metastable states and hysteresis. The qualitative features of the simulated hysteresis loops closely resemble our results and even the sizes of the loops are similar. Furthermore, the simulated and experimental loops evolve in the same way with temperature; roughly rectangular loops become narrower and more triangular as the temperature is raised and disappear slightly below the LVCP. At higher temperatures the simulated isotherms have finite slopes, as do our ex-

perimental ones. If there is an equilibrium liquid-vapor transition, it must be masked by the hysteresis loops at temperatures far from the LVCP and disappear before the hysteresis loops do.

Although the simulated aerogels all have porosities of 95% or less, the porosity dependence of the isotherms also qualitatively resembles the behavior in our experiments. Loops become more rectangular as the density of the gel decreases, and the disappearance of hysteresis occurs closer to the bulk critical temperature. Since the simulations which showed this behavior use mean field calculations, it does not appear that critical thermal fluctuations are needed to explain the evolution of the hysteresis or its disappearance below the bulk critical temperature. If true thermal critical behavior is observable for fluids in aerogel, then it must be very subtle. This is also consistent with the recent neutron scattering study of CO₂ in aerogel¹⁵ which did not see any evidence of a diverging coherence length near the LVCP.

Many of the features of our adsorption isotherms are similar to those associated with capillary condensation in denser media, despite the lack of well defined pores in aerogel. In dense media, fluid can be pictured as being adsorbed on the walls of archetypal pores (cylindrical, slit, or ink bottle, for example). As fluid is adsorbed, a liquid-vapor interface forms with a negative curvature which shifts the equilibrium conditions and causes liquid to condense below the bulk saturated vapor pressure. This behavior is described quantitatively by the Kelvin equation, which can be written as:

$$P_0 - P_v = -C\gamma \left(\frac{v_l}{v_v - v_l} \right) \quad (3)$$

where C is the curvature of the liquid-vapor interface, γ is the surface tension of the fluid, P_0 is the saturated vapor pressure at a given temperature, P_v is the pres-

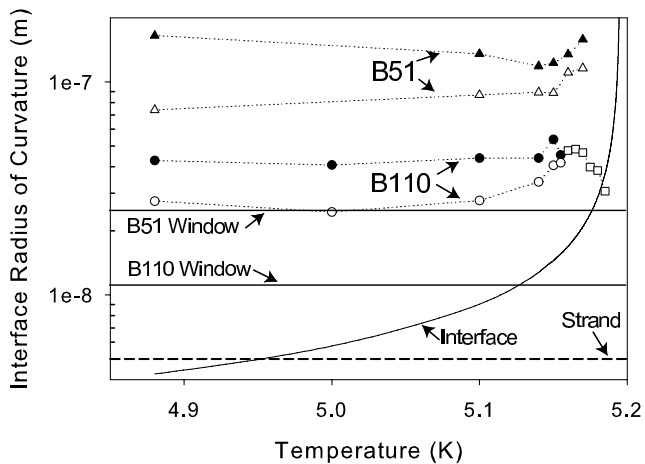


FIG. 17: Effective radii of curvature for the helium liquid-vapor interfaces during adsorption (solid symbols) and desorption (open symbols) in aerogels B110 (circles) and B51 (triangles), from the Kelvin equation. The approximate thickness of the aerogel strands and the bulk liquid-vapor interface thickness are included on the plot, as are the window sizes of cubic networks with densities equivalent to B110 and B51.

sure at which capillary condensation occurs, and v_l and v_v are the molar volumes of the liquid and vapor phases respectively. All of these terms are temperature dependent except for the curvature of the interface, which is assumed to remain well-defined and constant. However, aerogels are best described as a tenuous network of silica strands, not as a set of regular pores and it seems unlikely that condensation would involve a liquid-vapor interface with a constant negative curvature — the mean field simulations^{16,26} discussed above do not show evidence for a constant curvature interface.

The depression of the condensation pressure in our measurements (filling at $P/P_0 < 1$ in Figs. 7 to 15) does scale roughly with the bulk surface tension of helium, as one would expect for capillary condensation. If one assumes that condensation of helium in aerogels can be well described by the Kelvin equation then we can extract an effective curvature of the liquid-vapor interface which is responsible for the lower condensation pressure. To convert curvature to a radius one must assume a shape for the liquid-vapor interface, e.g. hemispherical. The effective radii for hemispherical liquid-vapor interfaces in our aerogels (B110 and B51) are shown in Fig. 17. The radii were extracted from the filling and emptying pressures using the Kelvin equation and assuming bulk values for surface tension and molar volumes. Also included in the figure are several other relevant length scales: the thickness of the aerogel strands, the thickness of the bulk liquid-vapor interface, and effective “window sizes” for models of aerogel as a cubic lattice of intersecting cylinders, with the cylinder thickness and sample density chosen to reflect our samples³⁶.

The average low temperature (i.e. less than 5.150K)

Sample	Branch	r
B110	Filling	43nm
	Emptying	28nm
B51	Filling	135nm
	Emptying	85nm

TABLE I: Effective radii of curvature of the liquid-vapor interface extracted from the Kelvin equation assuming a hemispherical meniscus.

values for the radius “r” extracted from the Kelvin equation are summarized in Table I. If the interface has the same shape during filling and emptying, then its effective radius of curvature must be roughly 50% larger on filling than emptying, but this difference more likely reflects different interface shapes during adsorption and desorption. For desorption it may be possible to interpret the effective radius of curvature as a “breakthrough radius” for the penetration of vapor into the aerogel voids, but it is unclear what the effective radius during adsorption could represent.

The thickness of a bulk liquid-vapor interface is given by³⁷ $L = 3.64\xi$ where L is the interface thickness and ξ is the fluid correlation length calculated as a function of reduced temperature, t , using $\xi = \xi_0 t^{-0.63}$ where³⁸ $\xi_0(^4He) = (1.8 \pm 0.3) * 10^{-10} m$. When the interface thickness is less than the thickness of the aerogel strands, it is reasonable to treat the helium as a bulk fluid with a well defined meniscus. However, once the interface exceeds the strand size, this picture breaks down. The aerogel strands may not pin the interface and the effective surface tension may differ from its bulk values. It is therefore surprising that the filling and emptying of the aerogels scales so well with bulk surface tension. Very close to the critical point, where hysteresis disappears, the bulk helium interface thickness is much larger than the strand diameter and is approaching the size of the average void in the aerogel. The effective interface radius of curvature changes rapidly in this temperature regime and it no longer makes sense to think of the system in terms of pores with a curved liquid-vapor interface. It is probably better to picture the aerogel as a random perturbation affecting the fluid phases in some averaged way.

Although our adsorption isotherms share many qualitative features with those in denser media, referring to the process as capillary condensation is somewhat misleading since aerogels do not have well defined pores. Instead, one can picture the helium as condensing around the strands and especially at their intersections. As adsorption proceeds, the fluid would fill regions with the highest strand density first, as in the simulations^{16,26}.

Since the aerogel silica backbone is so tenuous, it is easily deformed by small forces, including the surface tension that drives capillary condensation. In fact, one can see the effect of surface tension on the lower density aerogel in Fig. 8. The high pressure side of the B51 isotherm has

a negative slope after the completion of capillary condensation; this is due to surface tension compressing the sample and changing the area and separation of the capacitor plates.

We have studied the compression of aerogels by surface tension in more detail using a different technique⁴³. At 4.880K, aerogel B51 is compressed by up to 2% by helium's surface tension during desorption; B110, with its higher elastic constants, is compressed by less than 0.2% at the same temperature. In that study we were also able to measure the bulk moduli of our aerogels to be 0.4MPa and 0.04MPa for B110 and B51 respectively.

VI. SUMMARY

We have investigated the adsorption and desorption of helium near its LVCP in silica aerogel, a matrix with tunable density. Our measurements were made at temperatures far from the critical point, where a well defined liquid-vapor interface exists, and at temperatures close to the critical point where the fluid is expected to sense the aerogel in an averaged way. Nowhere did we see an unambiguous equilibrium first order transition, nor did

we see critical behavior dominated by thermal fluctuations. The very flat low temperature hysteresis loops in aerogel may reflect an underlying equilibrium phase transition in this system, but it is not experimentally accessible because of metastable states during filling and emptying. Many features of our isotherms could be described in terms of capillary condensation, although this picture becomes less applicable as the liquid-vapor critical point is approached. It is also unclear how the picture of capillary condensation caused by a liquid-vapor interface with a well-defined radius of curvature can be applied to aerogels, which have structure over a wide range of length scales. There is no evidence for a constant radius of curvature in the adsorbed fluid, and yet capillary condensation occurs over a very narrow pressure range — especially for very high porosity gels such as B51.

Acknowledgments

We would like to thank Moses Chan, Etienne Wolf, Norbert Mulders and Martin-Luc Rosinberg for helpful comments and discussions. Funding for this project was provided by NSERC.

* therman@phys.ualberta.ca

† beamish@phys.ualberta.ca

¹ J. Yoon, D. Sergatskov, J. Ma, N. Mulders, and M. H. W. Chan, *Physical Review Letters* **80**, 1461 (1998).

² M. H. W. Chan, K. I. Blum, S. Q. Murphy, G. K. S. Wong, and J. D. Reppy, *Physical Review Letters* **61**, 1950 (1988).

³ J. V. Porto and J. M. Parpia, *Physical Review B* **59**, 14583 (1999).

⁴ K. Matsumoto, J. V. Porto, L. Pollack, E. N. Smith, T. L. Ho, and J. M. Parpia, *Physical Review Letters* **79**, 253 (1997).

⁵ M. H. W. Chan, N. Mulders, and J. D. Reppy, *Physics Today* **49**, 30 (1996).

⁶ S. B. Kim, J. Ma, and M. H. W. Chan, *Physical Review Letters* **71**, 2268 (1993).

⁷ N. Mulders and M. H. W. Chan, *Physical Review Letters* **75**, 3705 (1995).

⁸ R. Schmidt, E. W. Hansen, M. Stöcker, and O. H. Akporiaye, Duncan Ellestad, *Journal of the American Chemical Society* **117**, 4049 (1995).

⁹ F. Brochard and P. G. de Gennes, *Journal de Physique - Lettres* **44**, L785 (1983).

¹⁰ P. G. de Gennes, *Journal of Physical Chemistry* **88**, 6469 (1984).

¹¹ B. J. Frisken, F. Ferri, and D. S. Cannell, *Physical Review E* **51**, 5922 (1995).

¹² M. Thommes and G. Findenegg, *Langmuir* **10**, 4270 (1994).

¹³ W. D. Machin, *Langmuir* **15**, 169 (1999).

¹⁴ M. Thommes, G. H. Findenegg, and M. Schoen, *Langmuir* **11**, 2137 (1995).

¹⁵ Y. B. Melnichenko, G. D. Wignall, D. R. Cole, and H. Frielinghaus, *Physical Review E* **69**, 057102 (2004).

¹⁶ F. Detcheverry, E. Kierlik, M. L. Rosinberg, and G. Tarjus, *Langmuir* **20**, 8006 (2004).

¹⁷ A. P. Y. Wong and M. H. W. Chan, *Physical Review Letters* **65**, 2567 (1990).

¹⁸ A. P. Y. Wong, S. B. Kim, W. I. Goldberg, and M. H. W. Chan, *Physical Review Letters* **70**, 954 (1993).

¹⁹ C. Gabay, P. E. Wolf, and L. Puech, *Physica B* **284**, 99 (2000).

²⁰ C. Gabay, F. Despetis, P. E. Wolf, and L. Puech, *Journal of Low Temperature Physics* **121**, 585 (2000).

²¹ T. Herman and J. Beamish, *Journal of Low Temperature Physics* **126**, 661 (2002).

²² T. Herman and J. Beamish, *Physica B* **329**, 431 (2003).

²³ J. Beamish and T. Herman, *Physica B* **329**, 340 (2003).

²⁴ J. R. Beamish and T. Herman, *Journal of Low Temperature Physics* **134**, 339 (2004).

²⁵ H. W. Tan and J. Beamish, *Physica B* **284**, 389 (2000).

²⁶ F. Detcheverry, E. Kierlik, M. L. Rosinberg, and G. Tarjus, *Physical Review E* **68**, 061504 (2003).

²⁷ D. Tulimieri, J. Yoon, and M. H. W. Chan, *Physical Review Letters* **82**, 121 (1999).

²⁸ G. Poelz and R. Riethmüller, *Nuclear Instruments and Methods* **195**, 491 (1982).

²⁹ T. M. Tillotson and L. W. Hrubesh, *Journal of Non-Crystalline Solids* **145**, 44 (1992).

³⁰ T. Herman, Ph.D. thesis, University of Alberta (2005).

³¹ G. C. Straty and E. D. Adams, *Review of Scientific Instruments* **40**, 1393 (1969).

³² E. W. Lemmon, M. O. McLinden, and D. G. Friend, in *NIST Chemistry WebBook, NIST Standard Reference Database Number 69*, edited by P. J. Linstrom and W. G. Mallard (National Institute of Standards and Technology, Gaithersburg MD, 20899 (<http://webbook.nist.gov>),

- 2003).
- ³³ R. Pelster, *Physical Review B* **59**, 9214 (1999).
- ³⁴ C. Gabay, Ph.D. thesis, CNRS - Grenoble (2001).
- ³⁵ K. Morishige and M. Shikimi, *Journal of Chemical Physics* **108**, 7821 (1998).
- ³⁶ G. W. Scherer, *Journal of Colloid and Interface Science* **202**, 399 (1998).
- ³⁷ D. Bonn and G. H. Wegdam, *Journal de Physique I* **2**, 1755 (1992).
- ³⁸ D. B. Roe and H. Meyer, *Journal of Low Temperature Physics* **30**, 91 (1978).
- ³⁹ Aerogel discs were cut with a high speed grinder (Micro Motor handpiece Model #MH-135, from Foredom Electric) fit with a diamond coated disc (Horico SuperDiaflex H635F220, supplied by Hopf, Ringleb & Co. GmbH&Cie.)
- ⁴⁰ "Maxwell[©] 2D," Ansoft Corporation
- ⁴¹ Mensor 1000psia gauge, Model 4040
- ⁴² The manual bridge was a General Radio model 1615-A. The automated bridge was an Andeen-Hagerling model AH2550A. Both bridges were operated at a frequency of 1kHz.
- ⁴³ T. Herman, J. Day, and J. Beamish, to be published